



## Assimilation and crystal accumulation in a mid-crustal magma chamber: the Sausfjellet pluton, north-central Norway

C.G. Barnes<sup>a,\*</sup>, G. Dumond<sup>a,1</sup>, A.S. Yoshinobu<sup>a</sup>, T. Prestvik<sup>b</sup>

<sup>a</sup>Department of Geosciences, Texas Tech University, P.O. Box 41053, Lubbock, TX 79409-1053, USA

<sup>b</sup>Department of Geology and Mineral Resources Engineering, Norwegian University of Science and Technology, N-7491 Trondheim, Norway

Received 17 July 2003; accepted 23 April 2004

### Abstract

The Sausfjellet pluton is made up of two intrusive units emplaced into high-grade metamorphic rocks of the Helgeland Nappe Complex of the Uppermost Allochthon in the Norwegian Caledonides. The eastern part of the pluton intruded marble and less voluminous calc-silicate and pelitic rocks. The western half is hosted predominantly by semi-pelitic migmatite with intercalated marble. Remelting of the migmatite during pluton emplacement occurred in a thermal aureole as much as 1000 m wide. The early gabbroic unit forms the southeastern part of the body; it consists of hornblende-bearing to hornblende-rich gabbro and diorite which is thought to have crystallized from an H<sub>2</sub>O-rich andesitic parental magma. The younger dioritic unit underlies the central and western parts of the pluton, as well as a zone as much as 200 m wide that separates the rest of the pluton from its host rocks (herein the “annular zone”). The interior or central zone of the dioritic unit is pyroxene diorite that is locally interlayered with anorthosite. The western and annular zones are, by comparison, mineralogically heterogeneous. They range from diorite to quartz monzonite and from biotite-bearing two- and three-pyroxene assemblages to biotite–hornblende assemblages. Neither rock type nor mafic assemblage is correlated with position in the pluton or proximity to a contact. Stopped blocks of a distinctive coarse-grained diorite, as well as pyroxene-rich calc-silicates, are present in the gabbroic unit and the central zone of the dioritic unit. The few stopped blocks observed in the western zone of the dioritic unit are predominantly quartz-rich gneiss. Chemical variation in the central zone of the dioritic unit is interpreted to result from accumulation of pyroxenes + plagioclase from an H<sub>2</sub>O-poor andesitic parent. These rocks have approximately constant  $\delta^{18}\text{O}$  of  $+6.6 \pm 0.2\%$  and lack evidence of in situ assimilation. Heterogeneities in the western and annular zones of the dioritic unit are reflected in variable, anomalously enriched incompatible element contents and in  $\delta^{18}\text{O}$ , which ranges from  $+6.7\%$  to  $+8.6\%$ . Petrologic models indicate that the magma parental to the central zone could also be parental to the western and annular zones. If so, evolution of the western and annular zone magma was by crystal accumulation and assimilation of metapelitic host rocks. As much as 20% of the mass of the western and annular zones can be ascribed to assimilated material, which apparently entered the magma by stopping. Therefore, the asymmetrical

\* Corresponding author. Fax: +1-806-742-0100.

E-mail addresses: [Cal.Barnes@ttu.edu](mailto:Cal.Barnes@ttu.edu) (C.G. Barnes), [gumond@geo.umass.edu](mailto:gumond@geo.umass.edu) (G. Dumond), [Aaron.Yoshinobu@ttu.edu](mailto:Aaron.Yoshinobu@ttu.edu) (A.S. Yoshinobu), [tore.prestvik@geo.ntnu.no](mailto:tore.prestvik@geo.ntnu.no) (T. Prestvik).

<sup>1</sup> Present address: Department of Geosciences, University of Massachusetts, 233 Morrill Science Center, Amherst, MA 01003-9297, USA.

zoning of the pluton is due to differences in host rock compositions and the relative ability of the magma to assimilate its host rocks.

© 2004 Elsevier B.V. All rights reserved.

*Keywords:* Diorite; Assimilation; Stopping; Caledonian; Norway

## 1. Introduction

The advent of isotopic fingerprinting showed that arc magmas commonly represent complex mixtures of mantle and crustal components (e.g., Kistler and Peterman, 1973, 1978; Taylor, 1980; DePaolo, 1981). The processes by which these components are incorporated into a magma, and their relative importance, are generally inferred from petrologic and geochemical studies of shallow plutons and volcanic rocks. A broad range of processes has been inferred in this manner. These include assimilation of crustal rocks by mafic magma, mixing of crustal and mantle magmas, and melting of a mixed source: crustal rocks previously “contaminated” by mantle-derived mafic intrusions. In general, such processes are inferred to occur in middle- to deep-crustal environments because of their higher ambient temperatures and slower cooling rates.

Although the chemical and isotopic evidence for crustal assimilation/mixing is unequivocal, the physical mechanisms by which hybridization occurs are less obvious. For example, does assimilation result from incorporation of stopped blocks in the magma? If so, is assimilation complete, with the entire block dissolved, or partial, leaving a refractory residue? If the latter, what is the fate of the residue and can it be recognized? Is assimilation actually the most reasonable process? Perhaps compositional trends that mimic assimilation are the result of episodic mixing of mantle-derived and crustally derived magmas. There is no reason why mixing + fractional crystallization cannot result in compositional trends that are very similar to assimilation + fractional crystallization (DePaolo, 1981). In view of the current debate concerning stopping (Marsh, 1982; Tikoff et al., 1999; Yoshinobu et al., 2003), evidence for stopping, and for its petrologic consequences, is likely to provide interesting constraints on the process.

In a companion paper (Dumond et al., *in press*), we report on the emplacement of the Sausfjellet

pluton, a laterally zoned dioritic and gabbroic body in the Norwegian Caledonides. The pluton was emplaced at middle crustal depths by a combination of stopping and ductile flow of its host rocks. Geologic and geochemical evidence indicates that lateral zoning developed, at least in part, because of differences in compositions of the host rocks. Parts of the pluton hosted by metacarbonate rocks show little chemical evidence of contamination by assimilation of host rocks, whereas parts hosted by metapelitic migmatites show trace element and isotopic evidence compatible with in situ host rock assimilation. In this paper, we focus on the petrologic history of the Sausfjellet pluton, the influence of its emplacement history on its petrologic development, and the effects of in situ assimilation as it interacted with its host rocks.

## 2. Geologic setting

The Sausfjellet pluton intrudes a nappe in the Helgeland Nappe Complex, which is the uppermost nappe complex in the Caledonides of north-central Norway. In the Velfjord area, the Helgeland Nappe Complex has been divided into four nappes. From structurally lowest, they are the Sauren-Torghatten, lower, middle, and upper nappes (Thorsnes and Løseth, 1991; Yoshinobu et al., 2002). The Sauren-Torghatten and middle nappes consist of basal ophiolitic rocks that are unconformably overlain by medium-grade metasedimentary sequences. The lower and upper nappes consist of migmatitic paragneiss, marble, calc-silicate rocks, and sparse amphibolite.

The nappes are separated by east-dipping shear zones. Displacement on these faults was originally in a west-vergent reverse sense. However, the shear zones between the Sauren-Torghatten and the lower nappe, and between the lower and the middle nappes show down-to-the-east, normal displacement reactivation (Yoshinobu et al., 2002).

Migmatization of pelitic and quartzofeldspathic rocks of the lower nappe accompanied upper amphibolite facies regional metamorphism and emplacement of a number of peraluminous (“anatectic”) granitic plutons. Metamorphism spanned the age range 477 to 468 Ma (Barnes et al., 2002; Yoshinobu et al., 2002) on the basis of U–Pb (zircon) ages of syn-metamorphic granites. From about 448 to circa 430 Ma (Yoshinobu et al., 2002; Nordgulen et al., 1993),

gabbroic to granitic plutons were emplaced; these constitute the principal mass of the Bindal Batholith. In the Velfjord region, this stage of Bindal magmatism began with emplacement of the dioritic Velfjord plutons (Fig. 1; Akset-Drevli,  $447.8 \pm 2.3$  Ma; Hillstadfjellet,  $447.0 \pm 3.2$  Ma; and Sausfjellet,  $445 \pm 11$  Ma; Yoshinobu et al., 2002) and the 447 Ma Andalshatten pluton (Nordgulen et al., 1993). Pressures of emplacement were in the 600 to 800 MPa range

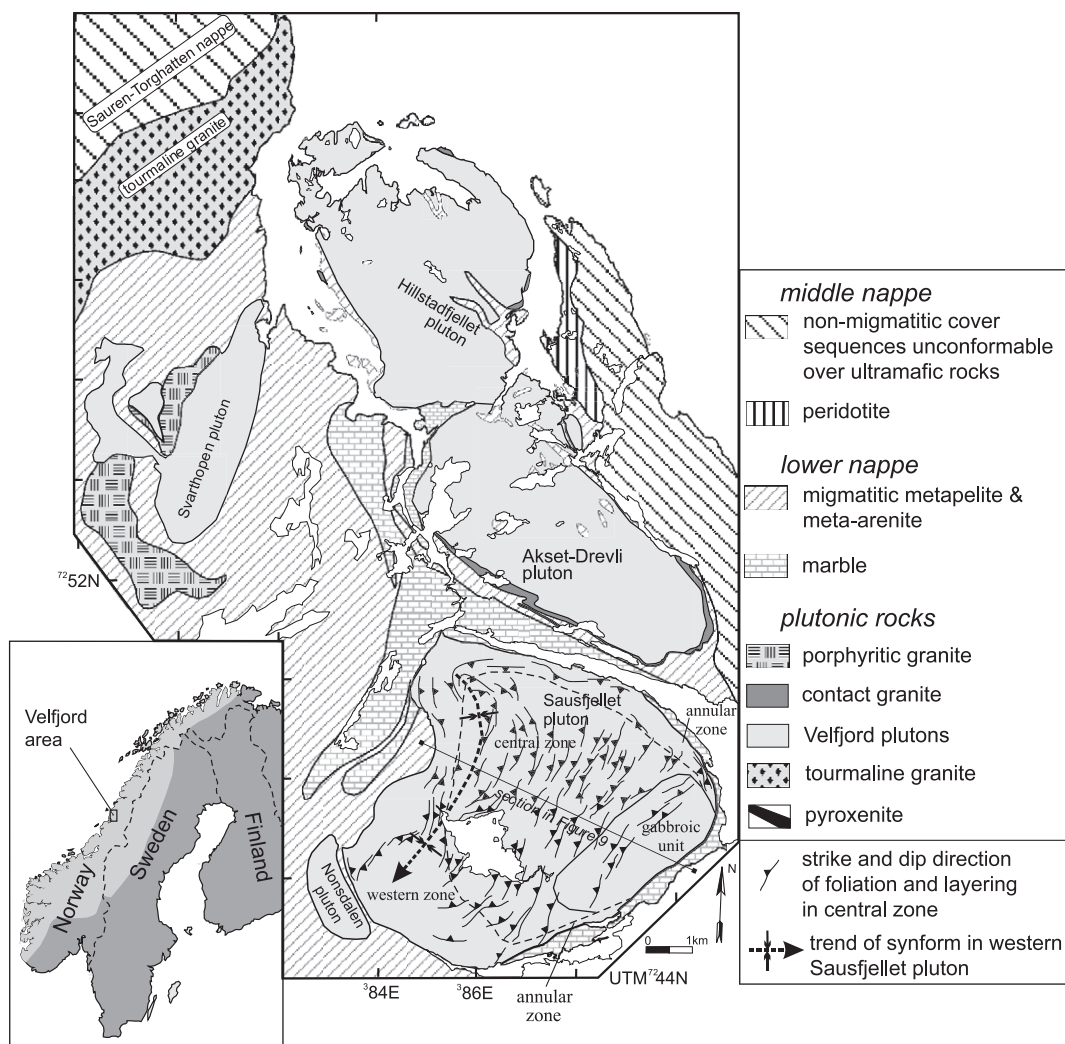


Fig. 1. Geologic setting of the Sausfjellet pluton. The contact between the high-grade host rocks of the Velfjord plutons and the eastern peridotite and non-migmatitic cover rocks is interpreted as a thrust fault with post-emplacment normal, down-to-the-east displacement. “Contact granites” resulted from emplacement of the Velfjord plutons; they are hybrids of leucosomes formed during melting of the pluton aureoles and dioritic magma.

(GASP thermobarometry and Al-in-hornblende barometry; Barnes and Prestvik, 2000).

The Sausfjellet pluton was emplaced after the Akset-Drevli pluton, as is shown by xenoliths of distinctive Akset-Drevli-type diorite in the Sausfjellet body (Dumond et al., in press). The small, undated Nonsdalen pluton flanks the southwestern side of the Sausfjellet pluton and is separated from it by a septum of marble and migmatitic gneiss. Geological relations cited below indicate that emplacement of the Nonsdalen pluton was coeval with emplacement of the Sausfjellet pluton.

The mechanisms of emplacement of the Sausfjellet pluton are detailed in Dumond et al. (in press). Three aspects of this process are noteworthy. First, a number of processes that included stoping, ductile flow in the host rocks, and foundering of the central-western portion of the pluton created space for the Sausfjellet magma. Second, the pluton was emplaced across a major lithologic boundary in the lower nappe that separates predominantly calcareous rocks to the east from pelitic and semi-pelitic rocks (migmatitic gneiss) to the west (Figs. 1 and 2). Thin bodies of pelitic gneiss that crop out along the northern and south-central contacts (Dumond et al., in press) are interpreted to result from ductile deformation of the aureole during emplacement. Third, contact metamorphism resulted in remelting of the adjacent pelitic and semi-pelitic gneisses in an aureole as much as one km wide (Barnes et al., 2002). In contrast to the layered (stromatic) fabrics of the regional migmatites, the contact migmatites are diatexites (migmatites lacking continuous internal structures). Some diatexites were mobilized into dike-like bodies that crosscut adjacent diatexite and locally intrude and brecciate the Nonsdalen pluton (Barnes et al., 2002). Contact migmatization was primarily by biotite-dehydration melting, which required minimum temperatures of circa 800 to 850 °C (Barnes and Prestvik, 2000). Mass balance calculations (Barnes et al., 2002) indicate that a minimum of 20% to 25% melt was produced in the host pelitic migmatites during contact melting.

The Sausfjellet pluton consists of two mappable units. The older “gabbroic” unit crops out in the southeastern part of the pluton. It consists of coarse- to medium-grained, massive to weakly foliated, hornblende-bearing to hornblende-rich gabbro and diorite (Table 1). Poikilitic hornblende is common and is

locally elongate in the plane of foliation. Xenoliths of calc-silicate rocks and diorite from the adjacent Akset-Drevli pluton are locally abundant in the gabbroic unit. The dioritic xenoliths reach 200 m in length (see Fig. 2 in Dumond et al., in press). Anastomosing epidote veins are present locally.

The younger “dioritic” unit is asymmetrically zoned from diorite to quartz monzodiorite (Fig. 2). The rocks are coarse- to medium-grained and are typically well foliated (Dumond et al., in press). Where visible, the contact between the gabbroic and dioritic units is sharp, and the grain size in the dioritic unit decreases from coarse to medium as the contact is approached.

On the basis of internal structures, mineral assemblages, and chemical compositions, the dioritic unit is divisible into three zones whose boundaries are entirely gradational (Fig. 2). The *central zone* forms the north-central part of the pluton (Fig. 2). It consists almost entirely of biotite augite opx diorite. Hornblende, if present, is an accessory mineral or is a deuteric replacement of pyroxene. Modal layering is widespread but only locally well developed in the northern part of the zone. It most commonly reflects variable proportions of pyroxene and plagioclase, with locally conspicuous anorthosite but rare pyroxenite. [See Dumond et al., in press for details of layering.]. Xenoliths of calc-silicate rocks and Akset-Drevli-type diorite reach 10 m in diameter and locally deform layering.

Dioritic rocks of the central zone grade westward, northward, and southward to dioritic and quartz monzodioritic rocks. Layering in the central zone dips beneath this gradational contact, so the gradation may also be upward to the west and southwest (Fig. 1). We refer to the broad area west of the central zone as the “western zone”. Two narrow (tens of meters to 200 m) arms extend from the western zone along the northern and southern margins of the pluton (Figs. 1 and 2). Because of the internal structure of these arms (see below) we refer to them as the “annular zone”. The transition from central zone to western and annular zones is marked by an increase in modal abundances of K-feldspar, quartz, amphibole, and biotite. Inverted pigeonite is locally present in the western zone and it is most common near the transition between central and western zones. Several transsects across the central/western zone boundary failed to

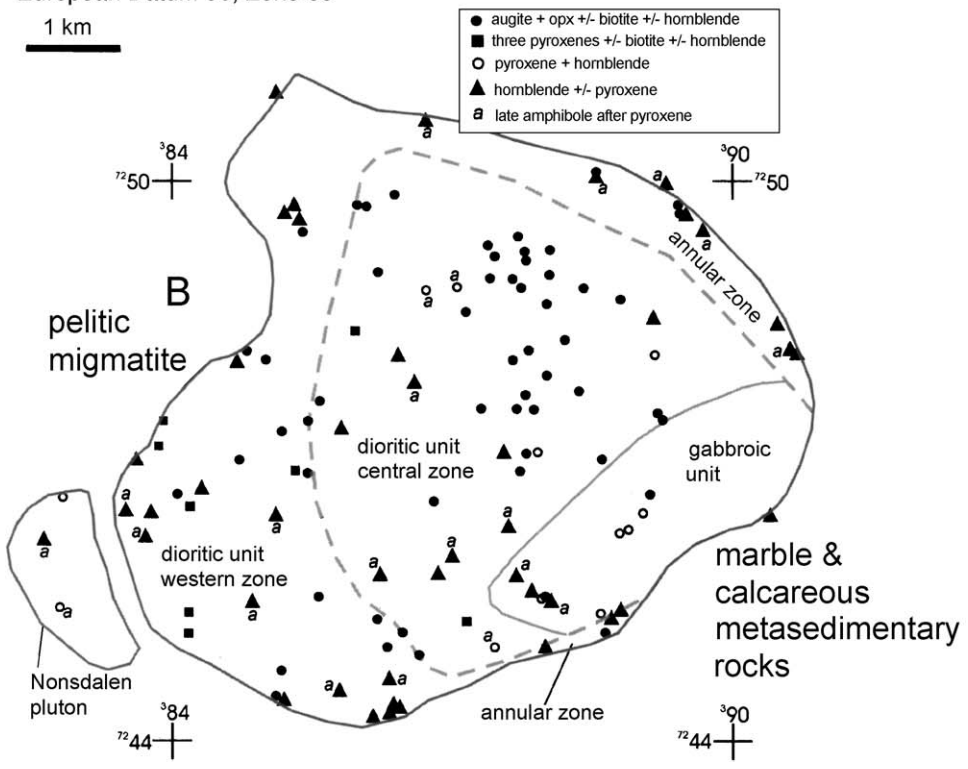
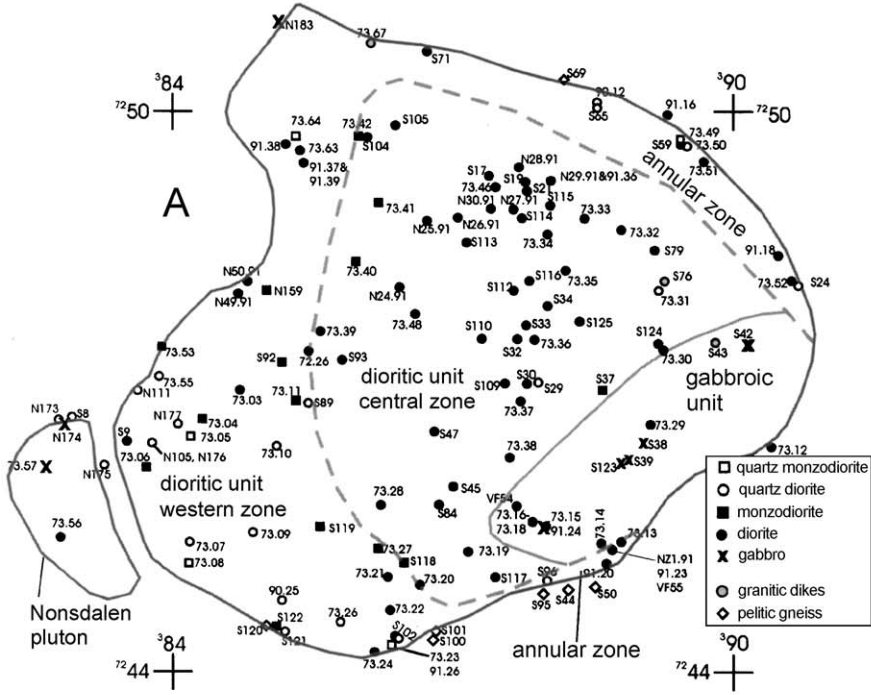
Table 1  
Summary of plagioclase compositions

Sample	Average (An%)	Core (An%)	Rim (An%)	Rock type	Notes
<i>Gabbroic unit</i>					
73.14	64.9	83	41	biotite augite opx hornblende gabbro	distinct An83-71 cores and An56-48 rims; cores may be An55
73.29	66.5	81	57	pyroxene gabbro	some oscillatory zoning; most crystals interstitial
73.30	56.0	81	47	opx augite gabbro	distinct calcic cores (An81-77); normally zoned rims (An60-47)
91.24	61.6	71	57	pyroxene hornblende gabbro	
S-42	76.1	78	66	hornblende opx augite gabbro	no zoning
<i>Samples evaluated as possible parental compositions</i>					
N30.91	44.9	49	42	biotite augite opx diorite	normal zoning
S-104	44.0	54	38	biotite augite opx diorite	large crystals are normally zoned
<i>Dioritic unit, central zone</i>					
73.19	53.8	63	50	bio-bearing augite opx diorite	some small calcic cores (An63); normally zoned rims
73.20	46.3	53	41	biotite augite opx diorite	normal zoning with weak core reversal
73.35	48.4	54	45	augite opx diorite	normal zoning
73.40	38.7	47	33	pigeonite augite opx monzodiorite	normal zoning
73.41	44.2	49	40	biotite augite opx monzodiorite	no zoning or weak normal
S-47	48.2	52	44	biotite-bearing augite opx diorite	norm zoning
S-124	48.1	54	44	augite opx diorite	weak normal or no zoning
S-116A	47.2	61	44	augite opx anorthosite	normal zoning; cores are An61 to 53
<i>Dioritic unit, western and annular zones</i>					
73.05	41.5	55	35	hblt biotite 3-pyroxene qtz monzodiorite	normal zoning; possible minor reversal at outer core
73.10	42.4	58	33	biotite hblt quartz diorite	distinct, small calcic cores with normal zoned rims
73.11	45.4	54	39	biotite augite opx monzodiorite	mostly normal zoning
73.21	44.5	49	40	augite opx diorite	no zoning or weak reversal at inner rim
73.27	40.7	47	36	biotite augite opx monzodiorite	normal zoning
73.65	41.4	43	39	epidote-bearing hblt biotite diorite	weak zoning
91.20	40.9	50	37	hblt biotite qtz monzodiorite	normal zoning
91.39	39.6	44	37	biotite augite opx monzodiorite	weak zoning
<i>Low-MgO dikes</i>					
91.22A	30.0	34	27	hblt epidote biotite quartz diorite	weak or no zoning
91.37	37.8	57	21	Kspar-phyric hblt-bearing biotite granite	sparse cores to An57; rims about An40 to 25
S-66	27.3	38	23	hblt biotite granite	distinct An38 core (resorbed); An26-23 rims

identify an intrusive contact, however a dike of western-zone type rock intrudes the central zone (sample N24.91; Fig. 2A). The western zone is typically massive to weakly foliated and contains

sparse, small (<20 cm diameter) calc-silicate and quartzofeldspathic xenoliths.

The annular zone is generally medium grained and moderately to strongly foliated (Dumond et al., in



press). Unlike the western and central zone, which have few dikes, the annular zone is characterized by medium- to fine-grained dioritic to quartz monzonitic dikes. These dikes strike sub-parallel to the pluton–host rock contact and some intrude the wall rocks (e.g., location 73.12; Fig. 2A).

Within the annular zone, magmatic foliations are commonly sub-parallel to the contact. Elsewhere in the dioritic unit, foliation and modal layering are folded in a synform that plunges shallowly to the southwest (Fig. 1). The foliation trajectory pattern cuts across the compositional zoning in the pluton (Fig. 1) and therefore postdates it. Asymmetric fabrics, tiled plagioclase laths, and magmatic C-S fabrics indicate top-to-the southwest normal shear parallel to foliation (Dumond et al., in press). Dumond et al. interpreted the synform and magmatic fabrics to indicate late-stage, southwest-directed foundering during magma chamber construction.

The Nonsdalen pluton consists of coarse- to medium-grained hornblende pyroxene gabbro and diorite. The unit is texturally similar to the gabbroic unit, but poor exposure and extensive deuteritic alteration limited our collection and description to a few samples.

### 3. Petrographic summary

The gabbroic unit is primarily opx augite amphibole gabbro that is characterized by cm-scale poikilitic amphibole. Oikocrysts enclose pyroxenes and plagioclase. Among the pyroxenes, the average Mg/(Mg + Fe) of augite is 0.73 and of opx is 0.67. The poikilitic amphibole is pargasite (average Mg/(Mg + Fe) = 0.64), which typically replaces augite. Plagioclase is generally interstitial. However, individual crystals have distinct cores (An<sub>83</sub> to An<sub>71</sub>) and rims (An<sub>60</sub> to An<sub>47</sub>). Epidote is a common secondary mineral in veins and replacing plagioclase and mafic minerals.

Diorite and anorthosite from the *central zone* of the dioritic unit are typically well foliated, with foliation formed by oriented plagioclase and pyroxenes (igne-

ous lamination). The texture can be described as hypidiomorphic granular or orthocumulate, in which opx, augite, and plagioclase are cumulus phases and biotite ± K-feldspar are intercumulus. Intercumulus K-feldspar is especially prominent in the anorthositic layers. Quartz, Fe–Ti oxides, and amphibole are accessory minerals or are absent. Unlike in the gabbroic unit, opx (Mg# 0.64 to 0.58) is more abundant than augite (Mg# 0.71 to 0.65). Sparse primary amphibole is edenitic, with Mg# 0.59. Deuteritic hornblende after pyroxene is locally present. The sequence of crystallization of mafic minerals is thought to be augite, opx, biotite ± amphibole. Plagioclase compositions range from An<sub>63</sub> to An<sub>33</sub>, with the range An<sub>54</sub> (core) to An<sub>44</sub> (rim) typical of most samples (Table 1). Thus, on the basis of plagioclase compositions these rocks could be classified either as gabbro norite or diorite. We choose to call them diorite, because the calcic cores occupy smaller volume than the more sodic mantles and rims.

The central zone grades into the *western and annular zones*. Centimeter-scale modal layering is present, especially in the northwestern part of the western zone, but is uncommon. The rocks are characterized by magmatic amphibole and by higher proportions of quartz and alkali feldspar than in the central zone. The mafic assemblage is quite variable and ranges from opx + augite + biotite, to opx + augite + inverted pigeonite + biotite ± amphibole, to amphibole + biotite ± (augite, opx, and inverted pigeonite). The three-pyroxene assemblage is most common in the transition between central and western zones (Fig. 2). The Mg# of pyroxenes is in the range 0.71 to 0.60 for augite, 0.54 to 0.52 for opx, and is 0.54 for inverted pigeonite. Amphibole is typically ferropargasite (Mg# from 0.50 to 0.33) but some samples contain edenite (Mg# 0.50 to 0.60). Plagioclase in the western and annular zones ranges from An<sub>58</sub> to An<sub>33</sub>. The most calcic compositions are of small cracked cores; individual samples are typically zoned from An<sub>54</sub> to An<sub>39</sub>. Normal zoning is common, but some crystals show single reversals of ~ 5% An

Fig. 2. Maps showing lithologic variation in the Sausfjellet pluton. (A) Distribution of rock types. The boundary between stage 1 and stage 2 is shown as a solid gray line and the boundary between zones of stage 2 with a dashed line. (B) Mafic mineral assemblages. An 'a' adjacent to a sample location indicates late-stage replacement of pyroxene by actinolitic amphibole. The dashed line in the aureole marks contact between predominantly calcareous host rocks to the east and predominantly metapelitic host rocks to the west.

component. It is noteworthy that the habits and compositions of plagioclase cores in the western and annular zones are essentially identical to those in the central zone, but plagioclase rim compositions are more albitic in the western and annular zones (Table 1; Dumond et al., in press).

Evolved dioritic to quartz monzodioritic dikes in the western and annular zones contain magmatic epidote, amphibole (ferropargasite), and biotite. Plagioclase compositions are in the An<sub>34</sub> to An<sub>27</sub> range (Table 1).

Interstitial Fe–Ti oxides are the most common accessory minerals in the pluton. Individual thin sections may contain magnetite or ilmenite or both. However, magnetite (oxy-exsolved) is predominant in the central zone and the gabbroic unit, whereas ilmenite is most common in the western and annular zones. Accessory apatite occurs throughout and ranges from robust subhedral prisms to interstitial grains. Zircon is present in the western and annular zones; in rare cases, it partly rims pyroxene.

Sample 73.05 from the western zone contains three coexisting pyroxenes + Fe–Ti oxides + quartz, which permits application of the QUILF algorithm (Lindsley and Frost, 1992; Frost and Lindsley, 1992). Analysis of backscatter images of the exsolved minerals was used to integrate the compositions of individual lamellae into pre-exsolution mineral compositions. These data were input into the QUILF4 program (Andersen et al., 1993). The calculated temperature and oxygen fugacity at 700 MPa are  $958 \pm 27$  °C and  $1.4 \pm 0.35$  log units above the fayalite–magnetite–quartz buffer, respectively.

In the gabbroic unit, calcic cores in plagioclase and the abundance of calcic amphibole are suggestive of relatively high H<sub>2</sub>O contents (e.g., Eggler, 1972; Beard, 1986). In contrast, the near absence of primary hornblende in the central zone of the dioritic unit suggests lower H<sub>2</sub>O contents. We take this contrast to indicate that parental magmas to the gabbroic unit and the central zone of the dioritic unit were compositionally distinct and unrelated to one another, at least at the level of emplacement.

The western and annular zones of the dioritic unit contain higher proportions of amphibole, much of which is prismatic. This suggests that H<sub>2</sub>O contents were higher than in the central zone magma and that hornblende was stable at temperatures well above the solidus.

#### 4. Geochemical variations

With few exceptions, samples of the Sausfjellet pluton range in SiO<sub>2</sub> content from 48 to 60 wt.% (Table 2; Fig. 3). The classification of Frost et al. (2001), shows the pluton to be magnesian and broadly calc-alkaline. Major and minor oxide concentrations vary widely, and compositional trends are poorly developed when plotted versus SiO<sub>2</sub>. MgO provides a better differentiation index and permits compositional distinctions to be made between various parts of the pluton. Compositions of gabbroic unit samples overlap with those of the dioritic unit. However, for a given MgO content, samples of the gabbroic unit have higher CaO and Al<sub>2</sub>O<sub>3</sub> (Fig. 3), and lower SiO<sub>2</sub> and Na<sub>2</sub>O.

The dioritic unit can be divided into two groups in plots of TiO<sub>2</sub> and total Fe versus MgO (Fig. 3). Dioritic samples from the central zone plot on a distinct trend with higher MgO and CaO than samples from the western and annular zones. Samples from the latter zones typically contain higher TiO<sub>2</sub>, K<sub>2</sub>O, Rb, Zr, Th, Y, and Ba contents (Figs. 3 and 4). The dikes that are part of the annular zone either plot among the compositions of their host rocks or extend the trend of western and annular zone samples to lower MgO contents (Figs. 3 and 4). Anorthositic samples from the central zone show the high Al<sub>2</sub>O<sub>3</sub> contents expected of plagioclase cumulates (Table 2). In addition, their K<sub>2</sub>O contents are higher than would be expected of plagioclase adcumulates.

Rare earth element (REE) patterns of dioritic rocks from the central zone show moderate light REE enrichment and anorthositic samples from the layered part of the zone show patterns characteristic of plagioclase cumulates (Fig. 5). Dioritic samples from the layered part of the zone have lower light REE than do samples collected near the boundary with the western zone (73.20 and 73.41) and diorites from the layered part of the zone commonly display positive Eu anomalies. Rare earth patterns of samples from the western and annular zones are uniformly light REE enriched (Fig. 5) and display slight negative Eu anomalies. No obvious correlation exists between total REE and differentiation; however the lowest REE abundances are observed in evolved, low-MgO dikes in the annular zone.

Nd isotope data (Barnes et al., 2002) show minor variation within the pluton. Two samples from the

Table 2  
Representative major and trace element compositions

Sample	Possible parents		Gabbroic unit					Dioritic unit central zone									
	N30.91	S-104	73.14	73.29	91.24	S-42	73.19	73.20	73.35	73.40	73.41	S-34A	S-47	S-115	S-116A	S-116B	S-124
SiO <sub>2</sub>	54.83	54.75	50.05	49.48	49.37	48.06	51.71	53.34	53.39	54.61	55.09	55.79	53.66	54.85	56.25	53.42	51.84
TiO <sub>2</sub>	0.52	0.63	0.83	1.04	0.73	0.31	0.51	0.69	0.46	0.78	0.73	0.20	0.54	0.11	0.20	0.52	0.70
Al <sub>2</sub> O <sub>3</sub>	18.74	18.52	17.14	19.14	18.79	22.82	12.62	16.93	13.83	19.61	20.49	25.84	18.54	26.95	25.41	16.68	20.65
Fe <sub>2</sub> O <sub>3</sub>	7.49	7.54	9.39	11.53	7.90	4.77	10.35	8.29	10.48	7.31	6.23	1.27	7.34	0.92	1.92	8.59	7.70
FeO	n.d.	n.d.	n.d.	n.d.	n.d.	n.d.	n.d.	n.d.	n.d.	n.d.	n.d.	n.d.	n.d.	n.d.	n.d.	n.d.	n.d.
MnO	0.13	0.13	0.17	0.17	0.12	0.08	0.21	0.15	0.20	0.12	0.08	0.02	0.13	0.01	0.03	0.16	0.14
MgO	5.32	4.83	7.91	4.92	7.94	5.99	11.96	6.99	10.14	3.26	3.55	0.63	5.75	0.47	1.12	7.54	4.27
CaO	8.81	7.88	11.12	9.49	12.97	15.43	10.48	8.93	9.31	7.49	8.36	9.22	8.79	10.14	9.37	8.81	9.51
Na <sub>2</sub> O	3.52	3.99	2.56	3.61	2.34	1.88	2.20	3.42	2.36	4.59	3.94	5.25	3.76	4.95	5.07	3.34	4.07
K <sub>2</sub> O	1.20	1.34	0.78	0.41	0.33	0.17	0.28	0.66	0.55	1.49	1.67	1.17	0.90	0.90	1.23	0.77	0.45
P <sub>2</sub> O <sub>5</sub>	0.12	0.18	0.03	0.63	0.09	0.04	0.08	0.26	0.08	0.26	0.22	0.06	0.09	0.05	0.09	0.07	0.22
LOI <sup>a</sup>	0.10	0.01	n.d.	n.d.	0.24	0.55	n.d.	n.d.	0.14	-0.11	0.34	0.26	0.07	0.35	0.15	0.00	0.08
Total	100.78	99.79	99.98	100.42	100.82	100.11	100.40	99.66	100.94	99.41	100.70	99.71	99.57	99.70	100.84	99.90	99.63
Mg# <sup>b</sup>	0.58	0.56	0.63	0.46	0.67	0.71	0.70	0.63	0.66	0.47	0.53	0.50	0.61	0.50	0.54	0.63	0.52
Be	n.d.	n.d.	n.d.	n.d.	n.d.	n.d.	n.d.	n.d.	n.d.	n.d.	n.d.	n.d.	n.d.	n.d.	n.d.	n.d.	n.d.
Cs	n.d.	1.72	n.d.	n.d.	n.d.	n.d.	n.d.	0.75	n.d.	n.d.	n.d.	0.41	n.d.	n.d.	n.d.	n.d.	n.d.
Rb	19	28.2	16	6	4	3	5	15	5	45	38	9	19	9	13	9	3
Sr	647	625	439	813	470	763	412	556	462	648	671	962	653	1075	961	613	896
Zr	100	112	68	10	67	59	27	47	59	111	123	30	80	33	71	60	55
Y	15	20.62	47	14	15	9	21	23.00	15	19	19	3.08	13	3	5	13	10
Nb	13	4.24	n.d.	n.d.	10	n.d.	n.d.	4.43	15	n.d.	15	0.86	n.d.	n.d.	n.d.	n.d.	n.d.
Ba	455	500	173	255	86	40	149	319	230	540	501	447	59	364	449	338	246
Sc	n.d.	23.7	39.6	18.8	n.d.	n.d.	46.1	30.2	n.d.	n.d.	n.d.	2.5	n.d.	n.d.	n.d.	n.d.	n.d.
V	166	141	159	238	158	96	164	135	175	182	152	20	150	13	31	133	160
Cr	50	15	298	43	158	80	179	72	209	8	15	11	87	dl	25	149	20
Ni	29	10	51	2	69	59	51	27	87	5	21	dl	37	dl	8	63	3
Cu	n.d.	12	22	25	33	39	10	15	n.d.	28	n.d.	dl	7	2	3	5	19
Zn	55	67	69	88	40	30	74	70	90	76	53	16	63	12	21	72	64
Co	23	25	n.d.	n.d.	39	26	n.d.	n.d.	50	23	17	dl	29	dl	4	35	21
Ta	n.d.	0.26	n.d.	n.d.	0.13	n.d.	n.d.	0.26	0.07	n.d.	0.23	0.06	n.d.	n.d.	n.d.	n.d.	n.d.
Hf	n.d.	2.02	n.d.	n.d.	1.32	n.d.	n.d.	1.59	0.89	n.d.	2.1	0.39	n.d.	n.d.	n.d.	n.d.	n.d.
U	n.d.	1.15	n.d.	n.d.	bd	n.d.	n.d.	0.58	0.19	n.d.	1.7	0.34	n.d.	n.d.	n.d.	n.d.	n.d.
Th	n.d.	4.11	n.d.	n.d.	n.d.	dl	n.d.	1.92	0.64	7	6.4	0.99	3	b.d.	b.d.	b.d.	b.d.
Pb	n.d.	11.81	n.d.	n.d.	n.d.	4	n.d.	8.43	15.0	n.d.	12.27	8	11	11	8	7	7
W	n.d.	n.d.	n.d.	n.d.	bd	n.d.	n.d.	n.d.	dl	n.d.	n.d.	n.d.	n.d.	n.d.	n.d.	n.d.	n.d.
La	n.d.	21.49	n.d.	n.d.	8.33	n.d.	n.d.	21.59	7.96	n.d.	30.7	12.22	n.d.	n.d.	n.d.	n.d.	n.d.
Ce	n.d.	40.50	n.d.	n.d.	21.4	n.d.	n.d.	42.10	21.3	n.d.	52.4	18.62	n.d.	n.d.	n.d.	n.d.	n.d.
Pr	n.d.	4.68	n.d.	n.d.	n.d.	n.d.	n.d.	5.02	n.d.	n.d.	n.d.	1.81	n.d.	n.d.	n.d.	n.d.	n.d.
Nd	n.d.	18.91	n.d.	n.d.	12.2	n.d.	27.32	21.05	9.77	n.d.	20.4	6.44	n.d.	n.d.	n.d.	n.d.	n.d.

C.G. Burnes et al. / Lithos 75 (2004) 389–412

(continued on next page)

Table 2 (continued)

	Possible parents			Gabbroic unit						Dioritic unit central zone							
Sm	n.d.	4.25	n.d.	n.d.	2.95	n.d.	2.92	4.97	2.71	n.d.	4.7	1.08	n.d.	n.d.	n.d.	n.d.	
Eu	n.d.	1.55	n.d.	n.d.	1.02	n.d.	n.d.	1.42	1.13	n.d.	1.5	1.42	n.d.	n.d.	n.d.	n.d.	
Gd	n.d.	3.84	n.d.	n.d.	n.d.	n.d.	n.d.	4.61	n.d.	n.d.	n.d.	0.83	n.d.	n.d.	n.d.	n.d.	
Tb	n.d.	0.60	n.d.	n.d.	0.46	n.d.	n.d.	0.72	0.44	n.d.	0.6	0.11	n.d.	n.d.	n.d.	n.d.	
Dy	n.d.	3.68	n.d.	n.d.	n.d.	n.d.	n.d.	4.34	n.d.	n.d.	n.d.	0.60	n.d.	n.d.	n.d.	n.d.	
Ho	n.d.	0.75	n.d.	n.d.	n.d.	n.d.	n.d.	0.87	n.d.	n.d.	n.d.	0.11	n.d.	n.d.	n.d.	n.d.	
Er	n.d.	2.02	n.d.	n.d.	n.d.	n.d.	n.d.	2.34	n.d.	n.d.	n.d.	0.30	n.d.	n.d.	n.d.	n.d.	
Tm	n.d.	0.30	n.d.	n.d.	n.d.	n.d.	n.d.	0.34	n.d.	n.d.	n.d.	0.04	n.d.	n.d.	n.d.	n.d.	
Yb	n.d.	1.94	n.d.	n.d.	1.05	n.d.	n.d.	2.16	1.4	n.d.	1.2	0.25	n.d.	n.d.	n.d.	n.d.	
Lu	n.d.	0.30	n.d.	n.d.	0.19	n.d.	n.d.	0.33	0.27	n.d.	0.19	0.04	n.d.	n.d.	n.d.	n.d.	
Dioritic unit																	
	Western and annular zones						Low-MgO dikes						Other dikes				
Sample	73.07	73.08	73.10	73.65	91.20	91.39	S-65	S-117	91.22A	N-159A	S-66	91.22B	N24.91				
SiO <sub>2</sub>	55.41	52.89	55.03	51.78	53.21	54.25	55.69	48.86	64.35	53.88	65.85	48.39	49.43				
TiO <sub>2</sub>	1.00	1.83	1.00	1.38	1.37	1.09	0.95	1.63	0.67	0.84	0.51	1.09	1.30				
Al <sub>2</sub> O <sub>3</sub>	16.95	15.74	17.82	19.39	17.81	17.21	17.23	19.41	17.32	19.12	16.32	19.06	19.26				
Fe <sub>2</sub> O <sub>3</sub>	9.07	11.17	8.74	9.43	2.88	9.49	7.67	11.02	0.61	8.08	3.72	10.49	10.15				
FeO	n.d.	n.d.	n.d.	n.d.	6.43	n.d.	n.d.	n.d.	3.91	n.d.	n.d.	n.d.	n.d.				
MnO	0.15	0.17	0.15	0.13	0.17	0.15	0.13	0.10	0.07	0.13	0.06	0.16	0.14				
MgO	4.20	4.10	4.34	3.75	4.54	4.80	3.87	4.15	1.82	2.88	1.14	5.38	5.46				
CaO	6.84	7.23	6.80	7.49	7.97	7.97	6.85	7.65	4.49	7.10	3.28	9.38	8.40				
Na <sub>2</sub> O	3.84	3.81	3.90	3.16	3.90	3.56	4.10	3.67	4.01	4.52	4.18	3.40	3.93				
K <sub>2</sub> O	2.00	1.98	1.77	2.75	0.93	1.74	1.82	2.15	1.96	2.27	3.63	2.02	1.78				
P <sub>2</sub> O <sub>5</sub>	0.24	0.94	0.13	0.57	0.66	0.27	0.33	0.90	0.23	0.53	0.19	0.59	0.41				
LOI <sup>a</sup>	−0.09	−0.23	0.54	0.73	0.16	0.03	0.43	0.54	0.30	1.20	0.31	0.65	0.79				
Total	99.61	99.63	100.22	100.56	100.03	100.56	99.05	100.09	99.74	100.55	99.19	100.61	101.05				
Mg <sup>#b</sup>	0.48	0.42	0.50	0.44	0.47	0.50	0.50	0.43	0.42	0.41	0.38	0.50	0.52				
Be	n.d.	n.d.	n.d.	n.d.	n.d.	n.d.	n.d.	5.7	n.d.	n.d.	n.d.	n.d.	n.d.				
Cs	n.d.	n.d.	n.d.	n.d.	n.d.	n.d.	n.d.	n.d.	3.17	n.d.	n.d.	1.75	2.56				
Rb	62	72	66	107	19	37	57	103	80	85	94	49	44				

Sr	522	533	611	812	635	545	560	598	586	839	649	1004	658
Zr	168	153	115	377	130	120	143	144	201	270	258	249	262
Y	31	39	20	25	23	25	25	35.0	16	28	18	27	27.96
Nb	n.d.	n.d.	n.d.	14	12	13	n.d.	14	15	n.d.	n.d.	11	8.16
Ba	578	726	389	1009	429	612	604	818	475	585	1113	875	486
Sc	n.d.	n.d.	n.d.	n.d.	n.d.	n.d.	n.d.	20.3	n.d.	n.d.	n.d.	n.d.	26.6
V	208	310	173	115	180	306	174	188	87	116	46	167	233
Cr	19	37	18	12	34	46	27	9	18	dl	dl	44	27
Ni	6	16	4	15	20	27	12	n.d.	18	dl	dl	19	21
Cu	21	31	9	12	7	15	11	28	2	9	9	8	75
Zn	91	100	98	109	93	80	84	103	60	91	67	109	91
Co	29	33	31	20	24	26	29	103	9	23	8	29	35
Ta	n.d.	n.d.	n.d.	0.91	0.62	n.d.	n.d.	n.d.	0.27	n.d.	n.d.	0.33	0.38
Hf	n.d.	n.d.	n.d.	8.58	2.57	n.d.	n.d.	n.d.	4.53	n.d.	n.d.	4.21	6.08
U	n.d.	n.d.	n.d.	2.29	1.56	n.d.	n.d.	n.d.	0.87	n.d.	n.d.	0.89	1.93
Th	12	15	8	19.41	3.87	n.d.	6	n.d.	6.46	17	36	6.96	8.02
Pb	18.0	20.0	15.0	n.d.	n.d.	n.d.	19	n.d.	17.0	18	25	12.89	12.54
W	n.d.	n.d.	n.d.	b.d.	b.d.	n.d.	n.d.	n.d.	b.d.	n.d.	n.d.	n.d.	n.d.
La	n.d.	n.d.	n.d.	44.7	43.3	n.d.	n.d.	n.d.	36.5	n.d.	n.d.	40.01	43.33
Ce	n.d.	n.d.	n.d.	112.8	101.5	n.d.	n.d.	n.d.	68.8	n.d.	n.d.	84.42	75.39
Pr	n.d.	n.d.	n.d.	n.d.	n.d.	n.d.	n.d.	n.d.	n.d.	n.d.	n.d.	10.30	9.39
Nd	n.d.	n.d.	n.d.	50.6	42.8	n.d.	n.d.	n.d.	24.8	n.d.	n.d.	41.19	38.23
Sm	n.d.	n.d.	n.d.	10.35	7.97	n.d.	n.d.	n.d.	4.28	n.d.	n.d.	7.59	7.95
Eu	n.d.	n.d.	n.d.	2.51	2.09	n.d.	n.d.	n.d.	1.16	n.d.	n.d.	2.21	2.09
Gd	n.d.	n.d.	n.d.	n.d.	n.d.	n.d.	n.d.	n.d.	n.d.	n.d.	n.d.	6.51	6.52
Tb	n.d.	n.d.	n.d.	0.86	0.81	n.d.	n.d.	n.d.	0.45	n.d.	n.d.	0.84	0.94
Dy	n.d.	n.d.	n.d.	n.d.	n.d.	n.d.	n.d.	n.d.	n.d.	n.d.	n.d.	5.26	5.37
Ho	n.d.	n.d.	n.d.	n.d.	n.d.	n.d.	n.d.	n.d.	n.d.	n.d.	n.d.	0.99	1.06
Er	n.d.	n.d.	n.d.	n.d.	n.d.	n.d.	n.d.	n.d.	n.d.	n.d.	n.d.	2.81	2.79
Tm	n.d.	n.d.	n.d.	n.d.	n.d.	n.d.	n.d.	n.d.	n.d.	n.d.	n.d.	0.36	0.40
Yb	n.d.	n.d.	n.d.	1.44	1.68	n.d.	n.d.	n.d.	1	n.d.	n.d.	2.61	2.43
Lu	n.d.	n.d.	n.d.	0.24	0.31	n.d.	n.d.	n.d.	0.18	n.d.	n.d.	0.40	0.39

n.d. indicates element not analyzed; b.d. indicates element below detection limits.

<sup>a</sup> A negative value for LOI indicates oxidation of iron during loss on ignition caused an increase in sample mass.

<sup>b</sup> Mg# is Mg/(Mg + Fe), where Fe is total Fe.

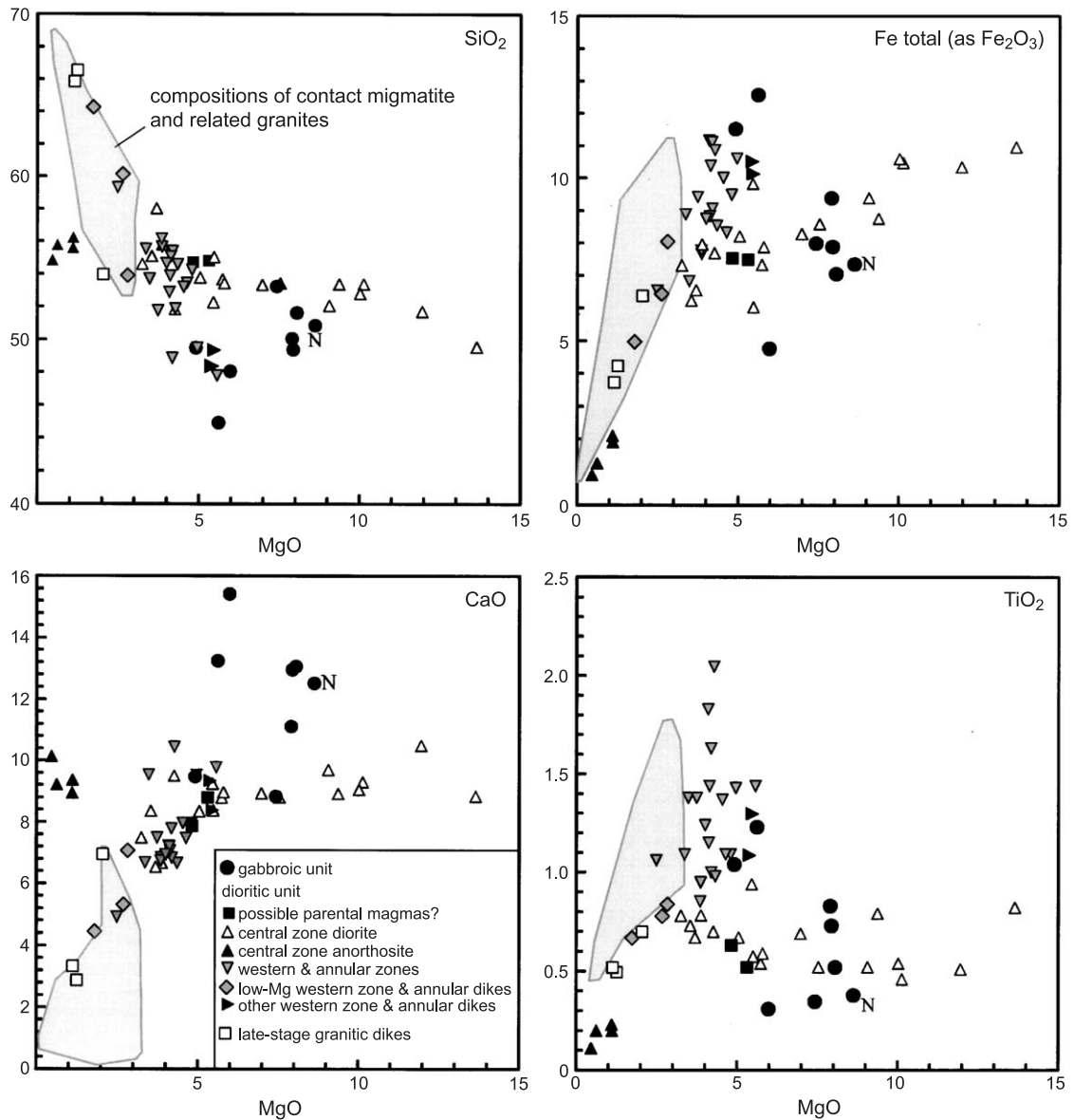
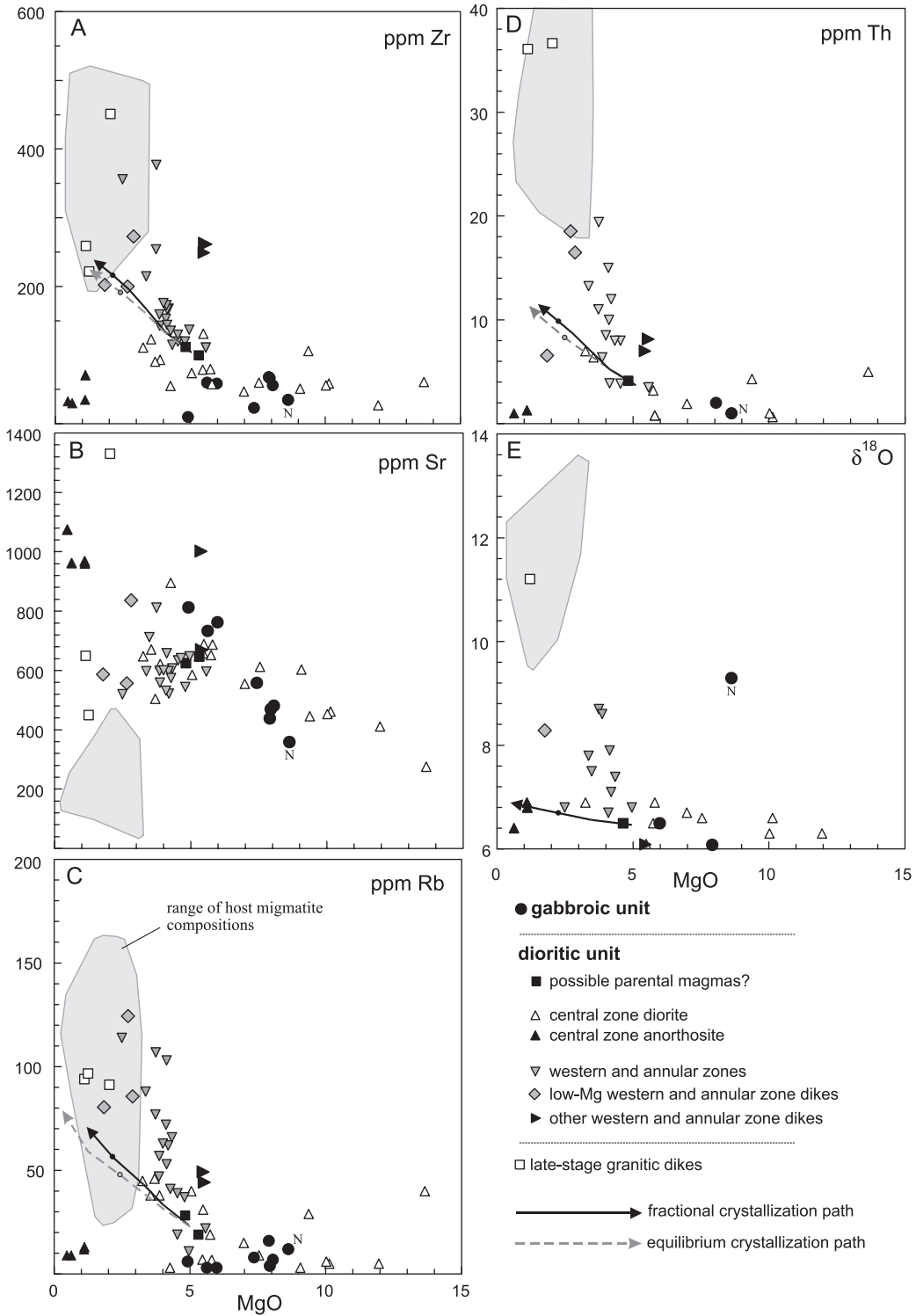


Fig. 3. Variation of representative major elements as a function of MgO content. The shaded region represents the range of compositions of host rock pelitic diatexites and contact granites.

gabbroic unit have  $\epsilon_{\text{Nd}}$  of 0.35 and 0.37 (calculated at 445 Ma), one sample from the central zone has  $\epsilon_{\text{Nd}}$  of 0.33, and six samples from the western and annular

zones have average  $\epsilon_{\text{Nd}}$  of  $-0.42 \pm 0.8$ . A larger data set is available for whole-rock oxygen isotope ratios (Table 3). Two samples from the gabbroic unit yield

Fig. 4. Representative trace element (in parts per million) and oxygen isotope diagrams. Oxygen data in per mil V-SMOW. The shaded region represents the range of compositions of host rock pelitic diatexites and contact granites. Solid arrows show fractional crystallization trends and dashed arrows show equilibrium crystallization trends for Zr, Rb, and Th in the western and annular zone. Note enrichments of these elements (and <sup>18</sup>O) in excess of that predicted by either type of crystallization.



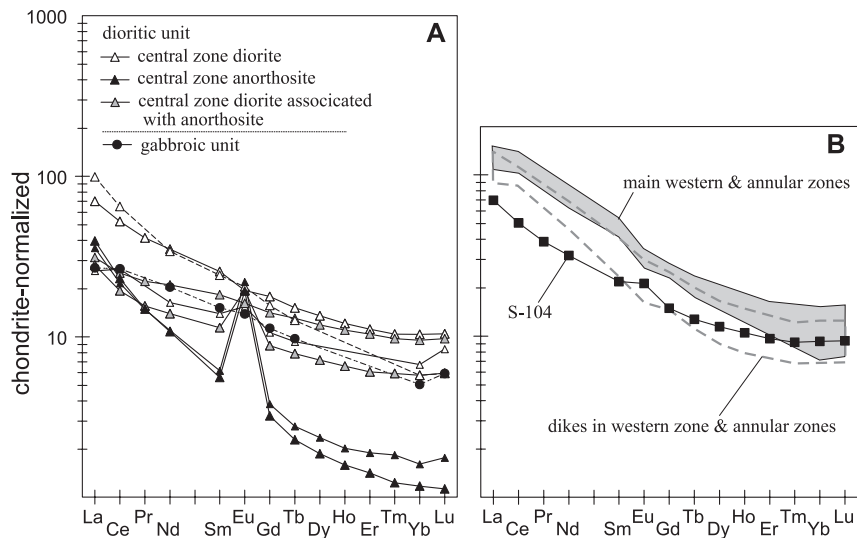


Fig. 5. Rare earth element patterns, normalized to chondritic abundances. (A) Stage 1 and samples from the central zone of stage 2. (B) Fields for rare earth element patterns of the western/annular zone of stage 2. Sample S-104 is one of two samples thought to be similar to the assumed parental magma. Note the slight positive Eu anomaly, which suggests that the sample may contain minor cumulus plagioclase.

$\delta^{18}\text{O}$  values of +5.9‰ and +6.5‰ and one sample from the Nonsdalen pluton has  $\delta^{18}\text{O}$  of +9.3. The central zone of the dioritic unit also has a limited range, from +6.1‰ to +6.9‰ (average  $+6.6 \pm 0.2\%$ ) (Fig. 4D). In contrast, western and annular zone samples range from +6.8‰ to +8.7‰. Four of these samples have  $\delta^{18}\text{O}$  values that overlap with those of the central zone within analytical uncertainty ( $<0.2\%$ ); seven others are distinctly higher. Within the western and annular zones,  $\delta^{18}\text{O}$  is not correlated with proximity to the pluton contact and is, at best, weakly correlated with differentiation.

## 5. Discussion

Our principal interests in this paper are the magmatic evolution of the pluton and its relationship to mechanisms of magma chamber construction. It is therefore necessary to estimate the compositions of parental magmas. We then discuss the compositional zonation in the dioritic unit and evaluate mechanisms that can explain such zonation.

The gabbroic unit and the central zone of the dioritic unit are each characterized by distinctive mafic assemblages and plagioclase compositions

(Table 1). This suggests that, although the rocks in each zone range widely in composition, these ranges are largely due to variable amounts of crystal accumulation.

The assemblage of augite, opx, and hornblende in the gabbroic unit is consistent with an  $\text{H}_2\text{O}$ -rich andesitic parental magma. This interpretation is also consistent with the presence of calcic plagioclase cores, which are characteristic of  $\text{H}_2\text{O}$ -rich magmas (e.g., Beard, 1986; Beard and Borgia, 1989). The parental magma was probably not basaltic, because olivine (or relict olivine) is lacking, because hydrous basaltic magmas precipitate extremely calcic plagioclase ( $>\text{An}90$ ; Beard, 1986) and because these probable cumulates still have comparatively low Cr ( $<300$  ppm) and Ni ( $<100$  ppm) contents.

In contrast, the magma parental to the central zone of the dioritic unit is interpreted to be an  $\text{H}_2\text{O}$ -poor andesite on the basis of the anhydrous cumulus assemblage (augite, opx, and plagioclase). The lack of hornblende is not due to a lack of intercumulus melt, because many central zone samples contain interstitial K-feldspar, quartz, and biotite. This magma was probably poorer in CaO than the parent of the gabbroic unit, as is indicated by the lower proportion of Ca-rich mafic silicates in the central zone, and

Table 3  
Oxygen isotope data

Sample	$\delta^{18}\text{O}$ (V-SMOW)	% yield
<i>Gabbroic unit</i>		
91.24	5.9	99.4
S-42.00	6.5	99.0
N104.99	9.3	104.7
<i>Dioritic unit, central zone</i>		
73.19	6.3	97.5
73.20	6.7	99.4
73.35	6.6	98.2
73.40	6.9	100.3
N26.91	6.1	98.9
S-34A.00	6.4	99.0
S-34B.00	6.3	98.6
S-47.00	6.5	99.1
S-112B.00	6.9	97.7
S-112C.00	6.9	97.6
S-116A.00	6.8	98.4
S-116B.00	6.6	97.6
<i>Dioritic unit, western and annular zones</i>		
72.26	6.5	100.9
73.05	7.8	97.6
73.07	7.1	99.4
73.08	6.7	98.4
73.10	7.4	100.9
73.39	7.5	98.3
73.52	6.8	97.2
73.55	7.9	98.3
73.65	8.7	95.8
91.26	7.6	98.8
S-65.00	8.6	100.5
<i>Dioritic unit, western and annular zone dikes</i>		
91.22A	8.3	99.2
N24.91	6.1	97.3
<i>Late stage two-mica tonalitic dike</i>		
73.60	11.2	97.5

particularly the abundance of orthopyroxene relative to augite.

The composition of magma parental to the western and annular zones is more difficult to determine, primarily because of the heterogeneity of this unit. This is seen in the distribution of hornblende, which is uneven (some samples lack hornblende), the range of  $\delta^{18}\text{O}$  values, and the range of incompatible element concentrations (Figs. 2 and 4; Tables 2 and 3). These characteristics suggest contamination of the western and annular zones by rocks with elevated  $\delta^{18}\text{O}$  values

and high concentrations of Zr, Rb, Th, Hf, etc. Despite these differences, plagioclase core compositions are virtually identical to those of the central zone (Table 1) and significant overlap exists among the compositions of mafic minerals.

## 6. Three models for the origin of compositional zonation in the dioritic unit

We consider three models concerning the origins of the distinct compositional groups in the dioritic unit. In the first model, the central and western + annular zones had similar, but distinct parental magmas that were unrelated at the level of emplacement. The central zone parent was  $\text{H}_2\text{O}$ -poor and gave rise to the locally layered, low- $\delta^{18}\text{O}$  rocks, whereas the western + annular zone parent was heterogeneous in  $\delta^{18}\text{O}$ ,  $\text{H}_2\text{O}$ , and incompatible elements at the time of emplacement and was not mixed by the emplacement process.

It is difficult to dismiss this model on geochemical grounds. Compositional heterogeneities in magma bodies are well known, but are typical of granitic magmas (e.g., Deniel et al., 1987) rather than dioritic ones. On a geologic basis, it is difficult to reconcile emplacement of two distinct magmas that share a contact that is gradational over at least 100 m width and several km long. No internal intrusive contacts were observed in spite of excellent exposure. One could envision convective mixing in two adjacent magma batches to explain the gradational contact. However, if convective mixing had occurred, then compositional heterogeneities in the western and annular zone magmas should have been destroyed (e.g., Clemens and Mawer, 1992).

The second model is one in which the dioritic unit represents emplacement of a single zoned magma body, whose zoning was acquired at a deeper structural level. As with the first model, we anticipate that transport of western and annular zone magmas should result in some degree of homogenization, particularly with regard to  $\text{H}_2\text{O}$  contents. It is also difficult to envision emplacement of a zoned magma in which layering developed only in the structurally lower parts.

The third model is one in which the magma parental to the dioritic unit was initially homogeneous, but underwent post-emplacement in situ differentiation

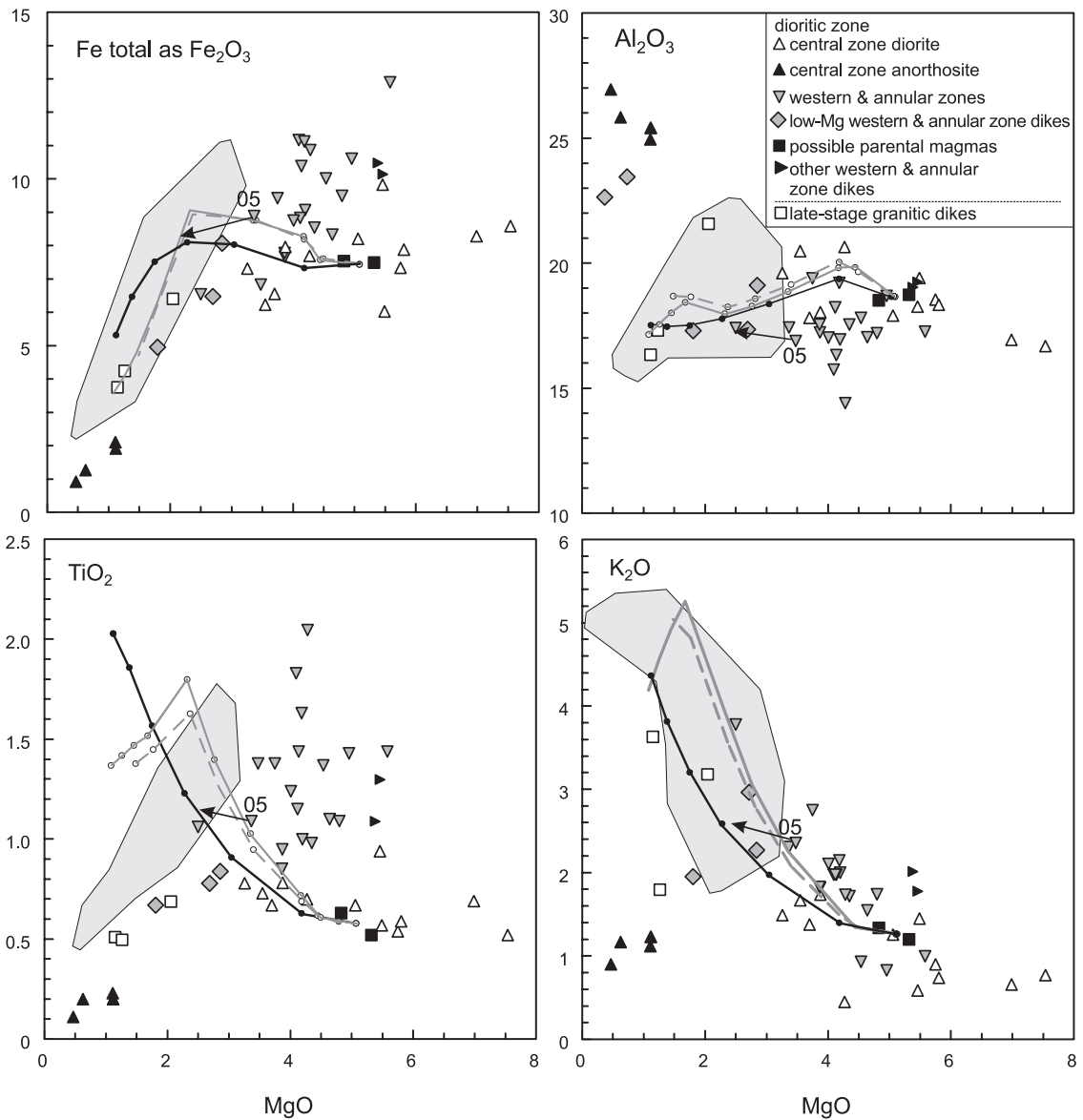


Fig. 6. Calculated liquid paths for stage 2 magmas. All calculations are for 700 MPa. The black line is the calculated trend from MELTS (Ghiorso and Sack, 1995) with  $fO_2$  one log unit above FMQ. The gray lines are calculations from PELE (Boudreau, 1999) with  $fO_2$  one (dashed) and two (solid) log units above FMQ. The arrow represents the direction of the liquid line of descent ( $fO_2 \sim 1$  log unit above FMQ) of a low-MgO, low-TiO<sub>2</sub> sample of the western/annular zone (sample 73.05; labeled “05”). The shaded field is the compositional range of host rock pelitic diatexites and contact granites.

so that the central zone magma was distinct from western and annular zone magmas. In this model, the “central zone” part of the magma behaved *chemically* as a closed system, with evolution controlled by crystal accumulation processes, whereas the western and

annular zone magmas underwent simultaneous crystallization and contamination. Contamination could have been by stoping, for which abundant field evidence exists (Dumond et al., *in press*), or by mixing of partial melts derived from the host rocks. This model

can explain the heterogeneous nature of the western and annular zones. However, before various mechanisms for contamination are explored, we consider the origin of major element variations in the dioritic unit.

## 7. Petrologic modeling

### 7.1. Introduction

Our approach to understanding compositional variation in the dioritic unit involved iteration between graphical analysis, numerical simulations of melt evolution using MELTS (Ghiorso and Sack, 1995) and PELE (Boudreau, 1999) programs, and mass balance calculations. We tried to determine (1) whether the compositional variation represented a liquid line of descent or the effects of crystal accumulation, (2) the probable composition(s) of parental magmas, and (3) whether the central and western zones could be related to a single parental composition.

### 7.2. Variation among central zone rocks

Central zone samples show a wide range of elemental concentrations (e.g., 17.5% to 0.47% MgO; 27% to 5% Al<sub>2</sub>O<sub>3</sub>; Table 2; Fig. 4), but share virtually the same mineral assemblage (see above). If these rock compositions represent a liquid line of descent, then one would expect, and numerical simulations demonstrate, that olivine should be stable in the mafic samples. One would also expect much less variability in Al<sub>2</sub>O<sub>3</sub>. This indicates that the central zone trend is predominantly the result of crystal accumulation.

A parental magma for the central zone trend should crystallize the observed cumulus assemblage (plagioclase, opx, augite) at 700 MPa and  $f_{O_2} \sim 1.5$  log units above FMQ. Among the samples considered, those with relatively high abundances of incompatible elements were thought most likely to represent melt compositions. Samples N30 and S-104 (Table 2) were chosen as likely candidates on the basis of Zr and Rb contents, and an average of their compositions (Table 2; 5.1% MgO) was used as input for numerical simulations. This composition is similar to an average of all analyses of dioritic zone samples. Water content was assumed to be less than 0.5 wt.%, because hornblende is lacking in many central zone samples.

For H<sub>2</sub>O contents from 0.2 to 0.5 wt.%, the calculated liquidus temperature is between 1250 and 1228 °C. A few degrees below the liquidus, both MELTS and PELE calculate a multiply-saturated liquid, with stable plagioclase, augite, and low-Ca pyroxene. If more mafic compositions are used, olivine is the liquidus phase and multiple saturation is reached tens to 100 °C below the liquidus. Calculated liquid paths show minor (MELTS) or strong (PELE) iron enrichment, as well as enrichment in TiO<sub>2</sub> (Fig. 6).

The simulations support the idea that the parental magma of the central zone was andesitic and was saturated in plagioclase and two pyroxenes at the time of emplacement or soon thereafter. If so, the anorthosites and MgO-rich diorites (Fig. 6) are the result of crystal accumulation. This conclusion was tested with least-squares major-element mass balance calculations (Bryan et al., 1969). The results (Table 4) show that anorthositic compositions can be explained by accumulation of ~ 70% plagioclase (An<sub>52</sub>) in the parental magma ± minor alkali feldspar and ilmenite. Dioritic compositions can be explained by accumulation of pyroxenes + plagioclase. With increasing MgO, the proportion of trapped liquid decreases (from ~ 50% to ~ 25%). The proportion of cumulus augite to total pyroxenes is about 0.4.

### 7.3. Variation among western and annular zone rocks

The trends calculated for the central zone parental magma typically intersect the compositional field of the western and annular zones. The intersection is near the low-MgO part of the main cluster of western and annular zone samples (Fig. 6; e.g., samples 73.05 and S65; Table 2). Most western and annular zone samples contain higher TiO<sub>2</sub> and total Fe (Fig. 6). No calculated fractionation trend showed sufficient enrichment in TiO<sub>2</sub> or Fe to explain the main cluster of samples, and the calculated trends extend to much higher K<sub>2</sub>O than is typical of western and annular zone samples (Fig. 6). This suggests that, as with the central zone, most western and annular zone samples contain cumulate phases. Major-element mass balance calculations (Table 4) support this assertion, and indicate that cumulus phases were plagioclase ± pyroxenes ± hornblende. In addition, accumulation of Fe–Ti oxides was required in nearly all calcula-

Table 4  
Examples of mass balance calculations of crystal accumulation

Rock	Interstitial melt	Interstitial melt (%)	ol	cpx	opx	plag	Kspar	mt	ilm	ap	$r^2$	plag/cpx	cpx/(opx + cpx)
Central zone samples with assumed parental compositions as interstitial melts													
<i>Dioritic unit, central zone</i>													
Dioritic rocks													
73.19	N30.91	60.7	15.1	22.5		1.7		0.5			0.235	0.08	1.00
			FO77			An <sub>63</sub>							
73.35	S-104	28.2		18.4	27.0	26.0						1.41	0.41
						An <sub>52</sub>					0.414		
73.35	N30.91	48.2		14.3	24.1	13.2					0.014	0.92	0.37
S-21B	S-104	25.9		13.2	25.8	33.8					0.258	2.56	0.34
						An <sub>63</sub>							
S-59	S-104	38.8		16.7	21.3	21.9						1.31	0.44
S-112B	S-104	49.4		7.7	10.5	30.7			1.1		0.366	3.99	0.42
						An <sub>52</sub>							
S-116B	S-104	37.8		11.0	17.7	32.1		0.8			0.026	2.92	0.38
						An <sub>52</sub>							
Anorthositic rocks													
S-112C	S-104	26.9				68.2	4.8		tr		0.344	na	na
						An <sub>52</sub>	Or <sub>82</sub>						
S-116A	S-104	25.4				70.8	4.9			0.1	0.101	na	na
						An <sub>52</sub>	Or <sub>82</sub>						
<i>Dioritic unit, Western and annular zone</i>													
73.55	73.05	89.4		4.4	3.8	2.1			0.01		0.119	0.48	0.54
						An <sub>52</sub>							
91.20	73.05	41.3		0.9	17.9	37.3			1.7	1.1	0.229	41.44	0.05
						An <sub>52</sub>							
N105	73.05	59.7			12	26.6			1.3	0.3	0.499	na	0.00
						An <sub>52</sub>							

Mineral abbreviations are: ol, olivine; cpx, augite; opx, orthopyroxene; plag, plagioclase; Kspar, K-feldspar; mt, magnetite; ilm, ilmenite; ap, apatite.

$r^2$  = sum of squares of residuals.

tions. The poor correlation of calculated to observed differentiation trends suggests that some process other than fractional crystallization is responsible for the decrease in TiO<sub>2</sub> and total Fe among the most evolved western/annular zone samples: the low-MgO dikes (Fig. 6).

Simulated differentiation models of magmas with the compositions of samples 73.05 and S-65 (with 0.5 wt.% H<sub>2</sub>O) produce liquidus phases of plagioclase (~ An<sub>50</sub>) augite, and pigeonite, but not Fe–Ti oxides. In other words, the numerical models do not show magnetite or ilmenite as cumulate phases, despite their abundance in many western/annular zone rocks (Fig. 3). If these minerals were not cumulate phases, then the high FeO and TiO<sub>2</sub> contents of most western zone samples could be the result of percolation of residual,

Fe-rich melts through the crystal pile and consequent precipitation of interstitial Fe–Ti oxides (e.g., Boudreau and McBirney, 1997). If this explanation is correct, it would additionally account for the compositions of low-MgO dikes in the western and annular zones: they crystallized from melts that were depleted of FeO and TiO<sub>2</sub> during percolation through the western zone mush.

If the zones within the dioritic unit share a common parental magma, and if the large compositional ranges in each zone are primarily due to crystal accumulation, then the calculated liquid line of descent involves no more than 50% crystallization. In Fig. 4, calculated trends for equilibrium and fractional crystallization are plotted for Zr, Rb, Th, and  $\delta^{18}\text{O}$ . We assumed that the trace elements were perfectly incompatible in

order to maximize closed-system enrichment. Fig. 4 shows that none of the trace element models match the compositional trends, and that Zr, Th, and Rb are enriched relative to closed-system crystallization. Similar enrichments are also observed for Ta (not shown) and  $\delta^{18}\text{O}$  (Fig. 4E).

Because closed system processes cannot explain these enrichments, we tested combined assimilation and fractional crystallization (AFC). Such processes can be modeled in a variety of ways (e.g., O'Hara and Herzberg, 2002) but are generally treated in terms of mass balance (e.g., Taylor, 1980; DePaolo, 1981) or energy balance (e.g., Spera and Bohrsen, 2001) problems. In the first case, the value of  $r$ , the ratio of the rate of assimilation/rate of crystallization, is fixed, whereas in the second it varies according to the thermal history of the modeled system. In addition, mass-balance models assume instantaneous assimilation.

The AFC models for the dioritic unit are illustrated in Fig. 7 in terms of Zr and  $\delta^{18}\text{O}$ . Oxygen isotope data were used because they do not require a priori estimates of bulk partition coefficients and because too few Nd isotope data are presently available. We recognize that  $\delta^{18}\text{O}$  can be reset by high-T subsolidus hydrothermal flow (e.g., Taylor and Forester, 1979). However, if pervasive hydrothermal alteration had occurred, then the variability seen in the western and annular zones should also be present in central zone samples. This is not the case (Figs. 4E and 7). Moreover, samples of the dioritic unit analyzed for  $\delta^{18}\text{O}$  lack any evidence for hydrothermal alteration. Widespread field evidence for hydrothermal exchange (e.g., epidote veins) was only seen in the gabbroic unit and the Nonsdalen pluton.

In Fig. 7, four mass balance models are shown (M1 through M4). The wide range of paths illustrates the effect of changes in bulk partition coefficient and the value of  $r$ . It is apparent that some combination of these variables will yield AFC paths that can explain most compositions of western and annular zone rocks. Cumulate rocks formed from melts that evolved along any of these paths would have compositions that plot to the left of the appropriate path. Therefore, if cumulates in the central zone represent part of an AFC process, they should show a much wider range of  $\delta^{18}\text{O}$ .

The energy balance calculations of Spera and Bohrsen (2001) assume that the host rocks must be

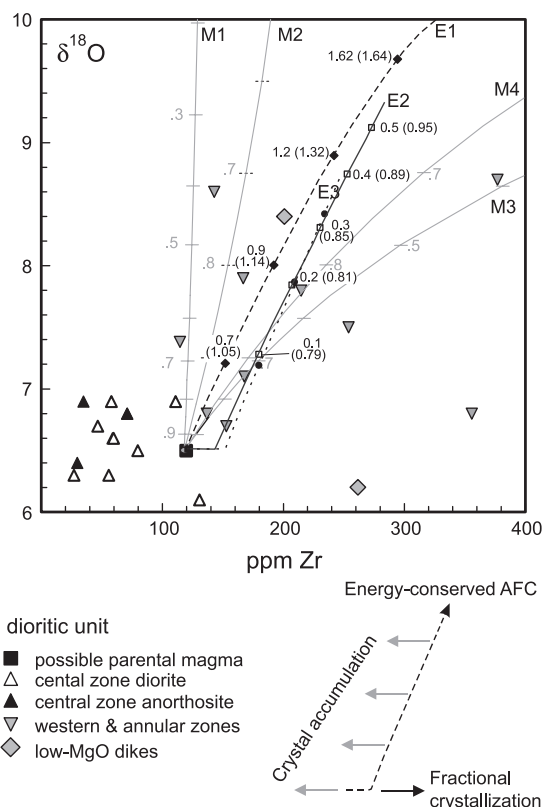


Fig. 7. Zr and  $\delta^{18}\text{O}$  compositions of stage 2 samples. The lines represent assimilation-fractional crystallization models for the western/annular zone. Models labeled with an M are mass-balance calculations. Tic marks represent fraction of liquid remaining. M1 and M2 are for Zr bulk partition coefficient of 1.5 and  $r$  values of 0.2 and 0.5, respectively. M3 and M4 are for Zr bulk partition coefficient of 0.1 and  $r$  values of 0.2 and 0.5, respectively. Models labeled with an E are energy balance calculations. Symbols along these curves are labeled with the mass fraction of assimilated material and, parenthetically, the instantaneous mass fraction of melt. Input parameters are given in Table 5.

partially molten before assimilation may occur, and that heat for host rock anatexis is transferred from the magma. Therefore, for assimilation to begin *at the time of emplacement* (path E1; input parameters in Table 5), the host rocks must be above their solidus. In contrast, use of host-rock temperatures appropriate for amphibolite-facies conditions (Table 5) results in melt evolution paths such as E2 and E3 in Fig. 7. These paths show initial differentiation by fractional crystallization alone (no change in  $\delta^{18}\text{O}$ ), followed by assimilation and an increase in  $\delta^{18}\text{O}$  and Zr contents.

Cumulate rocks associated with the first part of the path (no assimilation) would have compositions similar to the central zone, whereas cumulates that formed during assimilation would lie along or to the left of paths E2 or E3. Neither type of calculation explains the western and annular zone samples with high Zr contents and low  $\delta^{18}\text{O}$  values (Fig. 7). This may be a function of the wide range of compositions of the host rocks (Barnes et al., 2002) or may reflect local zircon accumulation.

Both types of calculation provide information about the mass of assimilated material. Samples of the dioritic unit with  $\delta^{18}\text{O}$  of  $\sim +8\%$  contain about 20% assimilated host rocks (by mass) according to energy balance calculations and about 10% according to mass balance calculations. We conclude that the enrichments in Th, Rb, Zr, Ta, and  $^{18}\text{O}$  in the western and annular zones of the dioritic unit are consistent with assimilation of the local pelitic host rocks. Assimilation of the observed stoped material (calc-silicate and dioritic rocks) cannot explain such enrichments.

It is clear from field evidence that stoping was an important process during crystallization of the central zone, because *dioritic* stoped blocks are embedded in

layering (Dumond et al., in press). However, if the pelitic contaminant modeled above entered the magma in the form of stoped material, there is no chemical evidence for it in central zone rocks. Such a process is still possible if the dioritic unit magma were vertically zoned, with a contaminated capping magma that did not mix with a lower magma that crystallized to form the precipitated central zone. This interpretation is generally consistent with the fact that the western zone is structurally higher than the layered central zone (assuming that layering was originally sub-horizontal; Dumond et al., in press). It does not explain the origin of the annular zone.

An alternative interpretation is that contamination of the western and annular zone magma was spatially restricted to the western part of the pluton  $\pm$  contact zones. In this case, we envision emplacement of homogeneous parental magma of the dioritic unit to be accompanied by stoping. Host (roof) rocks of the central zone (predominantly marble and diorite) were stoped into the magma but were refractory and difficult to assimilate (Fig. 8). In contrast, host rocks of the western part of the pluton (pelitic gneiss) were heated past their solidus during contact metamorphism. Stoped blocks of partially molten pelitic rocks would

Table 5  
Input parameters for energy-balance AFC calculations

Model number (Fig. 8)	E1	E2	E3
Liquidus $T$ of magma ( $^{\circ}\text{C}$ )	1240	1240	1240
Emplacement $T$ of magma ( $^{\circ}\text{C}$ )	1200	1200	1100
Liquidus $T$ of assimilated material ( $^{\circ}\text{C}$ )	1000	1000	
Initial $T$ of assimilated material ( $^{\circ}\text{C}$ )	800	500	500
Solidus $T$ of assimilated material ( $^{\circ}\text{C}$ )	725	725	725

All models used the following input parameters

	Magma	Bulk D	Assimilate	Bulk D	Isotope ratios	
					Magma	Assimilate
Oxygen					6.5‰	12‰
Zr	100 ppm	0.1	400 ppm	1.5		

Models were run with these input parameters in “linear” mode. The run was stopped at 900 $^{\circ}\text{C}$

(1) For model E2, the results indicate that assimilation would begin at about 1086  $^{\circ}\text{C}$ , at which point the ratio: (rate of change in mass of assimilate)/(rate of change in mass crystallized) jumps from 0 to  $\sim 1$ , and then increases gradually. At 900  $^{\circ}\text{C}$ , the mass proportion crystallized is about 0.65. The assimilation process causes a near-steady-state mass of magma from 1080 $^{\circ}$  to about 1000  $^{\circ}\text{C}$ , then an increase in the mass of magma. The mass proportion of assimilate at 1000  $^{\circ}\text{C}$  is about 0.2, which implies that 20% of the mass of the dioritic unit (closed system) can be “host rock”.  $\delta^{18}\text{O}$  at 1000 $^{\circ}\text{C}$  is about +8‰; Zr  $\sim 90$  ppm.

(2) The model was run again (E3) with the same parameters except an emplacement  $T$  of 1100  $^{\circ}\text{C}$  instead of 1200  $^{\circ}\text{C}$ . The results show the same pattern as at 1200  $^{\circ}\text{C}$ , but the beginning of assimilation is at 964  $^{\circ}\text{C}$ . In this case,  $\delta^{18}\text{O}$  values are +7.6‰ at 900  $^{\circ}\text{C}$ .

(3) An alternative model (E1) assumes that the host rocks were pre-conditioned by heat from the gabbroic unit. In this case, assimilation is essentially instantaneous and the mass of the magma increases continuously.

readily lose their interstitial melt and would probably be fragmented as melt from the dioritic magma replaced the original interstitial melt. Fragmentation would increase the surface area of the remaining solids and enhance further melting and dissolution into the host magma (e.g., Clarke et al., 1998).

This interpretation explains the abundance of stoped blocks in the central zone but the lack of

evidence for contamination. It also explains the evidence for contamination in the western and annular zones and the paucity of pelitic stoped blocks. Because the pelitic gneiss was partly molten prior to stopping and was soluble in western zone dioritic magma, it would probably produce small stoped blocks that were completely assimilated. Large stoped blocks of gneiss (10s to 100s of meters in diameter)

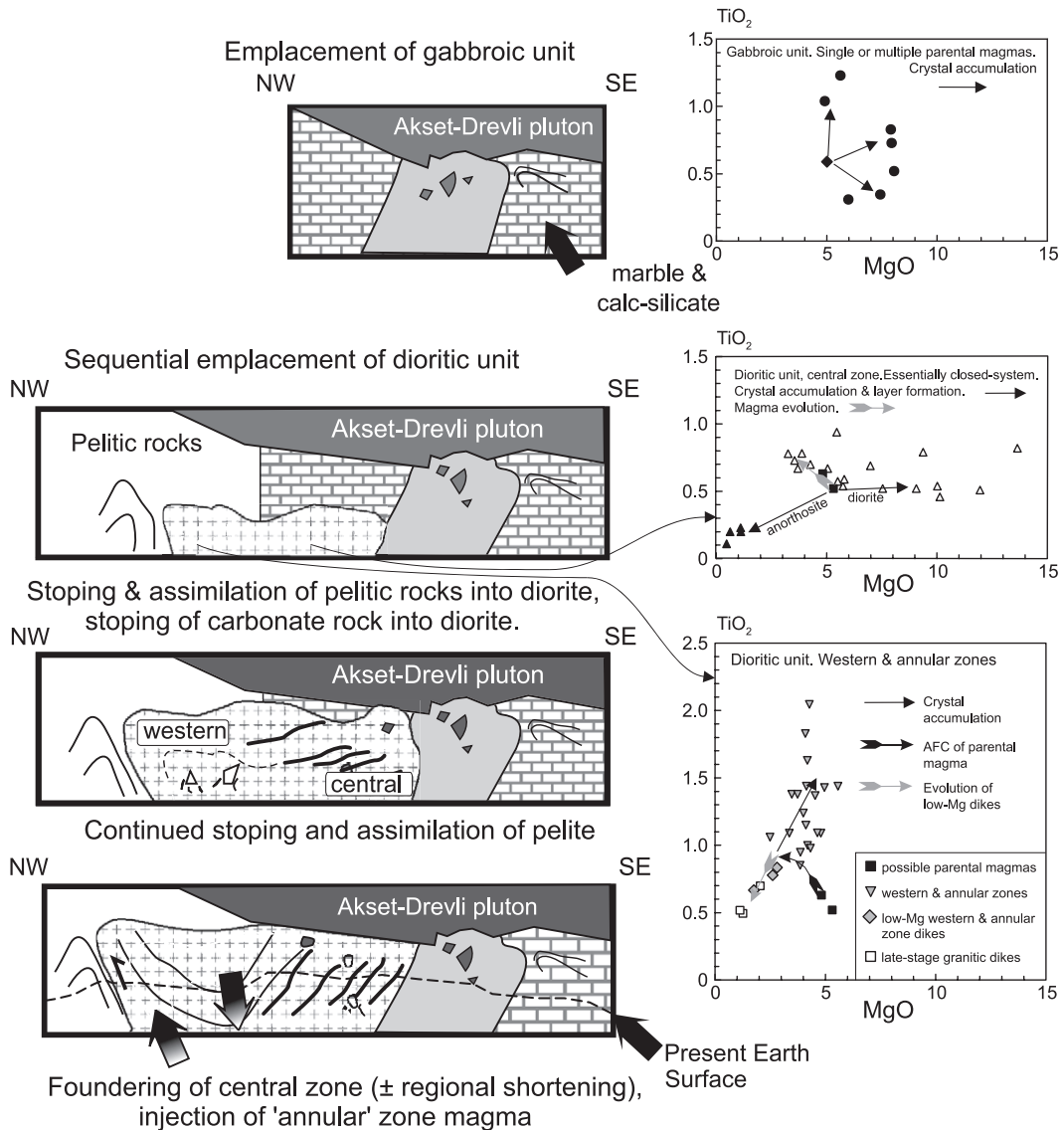


Fig. 8. Diagrammatic view of emplacement of the Sausfjellet pluton and evolution of the magma. Panels on the left are cross-sections to show the sequential emplacement of stages 1 and 2. Panels on the right illustrate the compositional variation in the magmas in terms of TiO<sub>2</sub> and MgO concentrations.

would be unlikely, because partial melting in the aureole made the gneiss mechanically weak.

This mechanism also explains the heterogeneity of the western and annular zones. As envisioned, stoping was a local process and stoped blocks ranged widely in chemical and isotopic composition (see Figs. 3 and 4). As long as convective mixing did not occur, each part of the western and annular zone magma would retain a signature of the amount of assimilation and the composition of the assimilated material. Further assessment of this idea clearly requires significant additional analytical detail, particularly in regard to Nd and Pb isotopes.

## 8. Preferred model of magmatic development of the Sausfjellet pluton

The first magma was H<sub>2</sub>O-rich andesite (gabbroic unit), which crystallized to hornblende-rich gabbro with calcic plagioclase. The wide compositional variation in this unit was primarily related to accumulation of variable proportions of plagioclase and mafic minerals (Fig. 8). Dumond et al. (in press) interpreted the gabbroic unit to underlie the dioritic unit, providing the base on which central zone cumulates were deposited. The sharp contact between the two units indicates that the gabbroic unit magma was unable to mix with the dioritic unit magma.

H<sub>2</sub>O-poor andesite was parental to the dioritic unit. This magma began to crystallize on its floor and, in what is now the central zone, developed a sequence of locally layered, dioritic to anorthositic cumulates. Stopping accompanied crystal accumulation, with stoped blocks trapped in the layered sequence (Fig. 8; Dumond et al., in press). Dioritic and calcareous stoped blocks had little effect on magma evolution because of their refractory compositions, so that evolution of magma in the central zone was by crystal–liquid separation (Fig. 8).

In contrast, stoped blocks of partially molten pelitic gneiss readily contaminated the magma into which they fell. The likely source for this pelitic material was adjacent to the western part of the pluton (Figs. 1, 2, and 8). Therefore, contamination due to stoping of pelitic rocks was limited to the western and annular zones. It is not certain whether this contamination was limited to the western part of the magma chamber or

whether it resulted in vertical zoning in which contaminated magma overlay uncontaminated magma. Our favored interpretation (Fig. 8) is that contamination by pelitic rocks was restricted to the western part of the magma chamber. If pelitic stoped blocks were already partly molten, then it is possible that their interstitial melt streamed out of the block and locally mixed with the surrounding magma. Because the proportion of stoped blocks was not the same everywhere in the magma, contamination was heterogeneous. Preservation of these heterogeneities suggest that convective overturn of western zone magma did not occur.

The geometry shown in Fig. 8 provides a mechanism by which annular zone and the low-MgO dike magmas could be contaminated and then emplaced. These magmas could represent evolved, fluid parts of the western zone that were episodically intruded between the wall rocks and cumulates of the central zone and the gabbroic unit (Fig. 8).

## 9. Conclusions

The Sausfjellet pluton was constructed from two discrete magma batches. An early, H<sub>2</sub>O-rich andesitic magma formed the gabbroic unit. A later, H<sub>2</sub>O-poor andesitic magma was parental to the dioritic unit. Stopping occurred throughout the history of the magma chamber. Calc-silicate and dioritic stoped blocks in the gabbroic unit and the central zone of the dioritic unit were too refractory to cause significant changes in magma composition. In contrast, contamination of the western part of the dioritic unit by partially molten metapelitic rocks resulted in elevated incompatible element concentrations and  $\delta^{18}\text{O}$  values. Stoped material constituted as much as 20% of the mass of this magma. Late-stage foundering in the interior of the pluton resulted in injection of western zone magma along pluton–host rock contacts to form the annular zone.

This work suggests that evidence for stoping as an emplacement mechanism cannot be limited to the physical presence of stoped blocks. Although refractory host rocks will be preserved, they may or may not be trapped at the level of exposure. More significantly, host rocks that are soluble in the host magma can be completely assimilated, leaving only geochemical evidence of their existence.

## Acknowledgements

This work benefited from the field and laboratory assistance of Melanie Barnes, from many conversations on local geology with Øystein Nordgulen and Roar Sandøy, and from reviews by Calvin Miller and Brian Robins. Support was provided by the National Science Foundation grant EAR-9814280 (Barnes), the Texas Tech University Research Enhancement Fund (Yoshinobu), the Nansen Foundation (Prestvik), and the Norwegian Geological Survey.

## References

- Andersen, D.J., Lindsley, D.H., Davidson, P.M., 1993. QUILF: a PASCAL program to assess equilibria among Fe–Mg–Mn–Ti oxides, pyroxenes, olivine, and quartz. *Computers and Geosciences* 19, 1333–1350.
- Barnes, C., Prestvik, T., 2000. Conditions of pluton emplacement and anatexis in the Caledonian Bindal Batholith, north-central Norway. *Norsk Geologisk Tidsskrift* 80, 259–274.
- Barnes, C.G., Yoshinobu, A.S., Prestvik, T., Nordgulen, Ø., Karlsson, H.R., Sundvoll, B., 2002. Mafic magma intraplating: anatexis and hybridization in arc crust, Bindal Batholith, Norway. *Journal of Petrology* 43, 2171–2190.
- Beard, J.S., 1986. Characteristic mineralogy of arc-related cumulate gabbros: implications for the tectonic setting of gabbroic plutons and for andesite genesis. *Geology* 14, 848–851.
- Beard, J.S., Borgia, A., 1989. Temporal variation of mineralogy and petrology in cognate gabbroic enclaves at Arenal volcano, Costa Rica. *Contributions to Mineralogy and Petrology* 103, 110–122.
- Boudreau, A.E., 1999. PELE—a version of the MELTS software program for the PC platform. *Computers and Geosciences* 25, 21–203.
- Boudreau, A., McBirney, A., 1997. The skaergaard layered series: Part III. Non-dynamic layering. *Journal of Petrology* 38, 1003–1020.
- Bryan, W., Finger, L., Chayes, F., 1969. Estimating proportions in petrographic mixing equations by least squares approximation. *Science* 163, 926–927.
- Clarke, D., Henry, A., White, M., 1998. Exploding xenoliths and the absence of ‘elephants’ graveyards’ in granite batholiths. *Journal of Structural Geology* 20, 1325–1343.
- Clemens, J.D., Mawer, C.K., 1992. Granitic magma transport by fracture propagation. *Tectonophysics* 204, 339–360.
- Deniel, C., Vidal, P., Fernandez, A., Peucat, J.-J., 1987. Isotopic study of the Manaslu granite (Himalaya, Nepal): inferences on the age and source of Himalayan leucogranites. *Contributions to Mineralogy and Petrology* 96, 78–92.
- DePaolo, D., 1981. Trace element and isotopic effects of combined wallrock assimilation and fractional crystallization. *Earth and Planetary Science Letters* 53, 189–202.
- Dumond, G., Yoshinobu, A.S., Barnes, C.G., in press. Mid-crustal emplacement of the Sausfjellet pluton, central Norway: ductile flow, stoping and in situ assimilation. *Geological Society of America Bulletin*.
- Eggler, D.H., 1972. Amphibole stability in H<sub>2</sub>O-undersaturated calc-alkaline melts. *Earth and Planetary Science Letters* 15, 28–34.
- Frost, B.R., Lindsley, D.H., 1992. Equilibria among Fe–Ti oxides, pyroxenes, olivine, and quartz: Part II. Application. *American Mineralogist* 77, 1004–1020.
- Frost, B.R., Barnes, C.G., Collins, W.J., Arculus, R.J., Ellis, D.J., Frost, C.D., 2001. A geochemical classification for granitic rocks. *Journal of Petrology* 42, 2033–2048.
- Ghiorso, M.S., Sack, R.O., 1995. Chemical mass transfer in magmatic processes: IV. A revised and internally consistent thermodynamic model for the interpolation and extrapolation of liquid–solid equilibria in magmatic systems at elevated temperatures and pressures. *Contributions to Mineralogy and Petrology* 119, 197–212.
- Kistler, R.W., Peterman, Z.E., 1973. Variations in Sr, Rb, K, Na, and initial Sr<sup>87</sup>/Sr<sup>86</sup> in Mesozoic granitic rocks and intruded wall rocks in central California. *Geological Society of America Bulletin* 84, 3489–3512.
- Kistler, R.W., Peterman, Z.E., 1978. Reconstruction of crustal blocks of California on the basis of initial strontium isotopic compositions of Mesozoic granitic rocks. U.S. Geological Survey Professional Paper 1071 (17 p.).
- Lindsley, D.H., Frost, B.R., 1992. Equilibria among Fe–Ti oxides, pyroxenes, olivine, and quartz: Part I. Theory. *American Mineralogist* 77, 987–1003.
- Marsh, B.D., 1982. On the mechanics of diapirism, stoping and zone melting. *American Journal of Science* 282, 808–855.
- Nordgulen, Ø., Bickford, M., Nissen, A., Wortman, G., 1993. U–Pb zircon ages from the Bindal Batholith, and the tectonic history of the Helgeland Nappe Complex, Scandinavian Caledonides. *Journal of the Geological Society (London)* 150, 771–783.
- O’Hara, M.J., Herzberg, C., 2002. Interpretation of trace element and isotope features of basalts: Relevance of field relations, petrology, major element data, phase equilibria, and magma chamber modeling in basalt petrogenesis. *Geochimica et Cosmochimica Acta* 66, 2167–2191.
- Spera, F., Bohron, W., 2001. Energy-constrained open-system magmatic processes I: General model and energy-constrained assimilation and fractional crystallization (EC-AFC) formulation. *Journal of Petrology* 42, 999–1018.
- Taylor Jr., H.P., 1980. The effects of assimilation of country rocks by magmas on <sup>18</sup>O/<sup>16</sup>O and <sup>87</sup>Sr/<sup>86</sup>Sr systematics in igneous rocks. *Earth and Planetary Science Letters* 47, 243–254.
- Taylor Jr., H.P., Forester, R.W. 1979. An oxygen and hydrogen isotope study of the Skaergaard Intrusion and its country rocks: a description of a 55-m.y. old fossil hydrothermal system. *Journal of Petrology* 20, 355–419.
- Thorsnes, T., Løseth, H., 1991. Tectonostratigraphy in the Velfjord-Tosen region, southwestern part of the Helgeland Nappe Complex, Central Norwegian Caledonides. *Norges Geologiske Undersøkelse Bulletin* 421, 1–18.

- Tikoff, B., St. Blanquat, M., Teyssier, C., 1999. Translation and the resolution of the pluton space problem. *Journal of Structural Geology* 21, 1109–1117.
- Yoshinobu, A.S., Barnes, C.G., Nordgulen, Ø., Prestvik, T., Fanning, M., Pedersen, R.-B., 2002. Ordovician magmatism, deformation, and exhumation in the Caledonides of central Norway: an orphan of the Taconic orogeny? *Geology* 30, 883–886.
- Yoshinobu, A.S., Fowler, T.K., Paterson, S.R., Llambias, E., Sato, A., Tickji, H., 2003. A view from the roof: magmatic stoping in the shallow crust, Chita pluton, Argentina. *Journal of Structural Geology* 25, 1037–1048.